IOP Publishing Measurement Science and Technology
Meas. Sci. Technol. **35** (2024) 105024 (10pp) https://doi.org/10.1088/1361-6501/ad63c3

# Gap measurement method based on projection lines and convex analysis of 3D points cloud

**Wei Pan[1], Bin-feng Jiang[2], Wen-ming Tang[3], Fu-pei Wu[4,*] and Sheng-ping Li[4]**

[1] Department of R&D, OPT Machine Vision Tech Co., Ltd, Dongguan 523853, People's Republic of China
[2] Department of R&D, Nordkette(SuZhou)Intelligent Equipment Co.,Ltd., SuZhou 215100, People's Republic of China
[3] School of Intelligent Manufacturing and Equipment, Shenzhen Institute of Information Technology, Shenzhen 518172, People's Republic of China
[4] School of Engineering, Shantou University, Shantou 515063, People's Republic of China

E-mail: wufupei@163.com

Received 27 April 2024, revised 8 July 2024
Accepted for publication 16 July 2024
Published 25 July 2024

**Abstract**

Accurate measurement of the gap between the lower surface of the relay and the ground is critical for ensuring the quality of the finished product. Traditional gap measurement methods have some shortcomings, such as low accuracy, poor robustness, and loss of depth clues in obscured areas. In this study, a novel gap measurement method based on computer vision is proposed, which includes a projection line model based on guided filtering and a 3D surface point cloud model based on a three-dimensional plane reference. The relay gap was measured by calculating the projection lines of the upper and lower surfaces of the gap with an error of $\pm$ 0.016 mm. A 3D point cloud model captures the key features of the underside of the relay through image processing techniques, and combines convex hull and centroid estimation to construct a three-dimensional reference plane for the gap, which could achieve high-precision, real-time measurement of the gap (with an error less than $\pm$ 0.0087 mm). The experimental measurement results show that the proposed method is better than the SelfConvNet method, which has a high measurement accuracy and strong anti-interference ability, and an accuracy rate of up to 99.5% in factory relay quality inspection experiments.

Keywords: computer vision, relay gap, guided filtering, projection lines, 3D convex hull

## 1. Introduction

Relays are widely used control devices in industrial production for remote control, communication, automatic control, mechatronics, and power electronic equipment [1–3]. The gap between the lower surface of relay and the ground represents a critical factor affecting the quality of relay products, where the quality significantly influences the conductivity and reliability of relays.

The common displacement sensors are eddy current type, inductive type, capacitive type, and photoelectric type. The eddy current sensor needs to be customized according to the shape of the measured object, and the cost is relatively high [4]. Conditions such as temperature fluctuations, humidity, and the presence of electromagnetic interference will affect the inductive distance sensor's accuracy and reliability. These environmental factors will lead to false readings or sensor malfunction [5], so it is not often used in relay system. Capacitive distance sensor is a noncontact sensor with simple structure and low cost, but it requires high-voltage power supply and has a large nonlinear error [6]. The photoelectric distance sensor

* Author to whom any correspondence should be addressed.

measures the displacement of the object according to a photoemission principle of the photocell. The photoelectric position sensor has high sensitivity, high resolution, and high speed, while its anti-interference ability to ambient light is poor [7].

Optical measurement offers advantages such as noncontact, fast processing speed, high detection accuracy, and strong adaptability. Numerous research achievements have been extensively applied to the detection field. For instance, Jing [4] proposed two non-contact measurement methods for levitation gaps based on computer vision in 2022, where the Pixel Area model has high measurement speed but low accuracy, while the SelfConvNet model has high accuracy but low speedy. Comparing with 2D measurements' methods, 3D measurements can provide more comprehensive structural information, facilitating precise measurements at multiple angles. For example, Srimontriphakdi [8] proposed a non-contact method for evaluating the top tension and bending stiffness of large cable-stayed objects using three-dimensional laser scanning data from ground-based laser scanners. However, the disorder and sparsity of point cloud data result in a time-consuming measurement process, which highlights the need for a more efficient processing method. As a fundamental unit of computational geometry, the convex hull, owing to its high computational efficiency and ease of implementation, has been widely used in mesh generation, clustering analysis, and image processing, including object detection [9], object recognition [10], and fault diagnosis [11], and in the measurement field, such as Norris [12], who achieved rapid and accurate measurement of human size through an improved convex hull algorithm. In a word, 2D measurements' methods usually constrained by the limitations of dimensions loss struggle to meet the accuracy requirements for measuring the gap beneath the surface of the relays, while the speed of normal 3D measurements also needs to be improved, which will significantly improve the output and economic benefits.

Considering the problems of traditional methods in measuring the gap of relay system, this paper introduces a gap measurement method based on projection lines and convex analysis of 3D points. Projection lines and surface point clouds were used to describe the relay gap and subsequently establish methods for the detection and measurement of the gap. The efficacy of the proposed method was validated through experimentation. The primary contributions of this study are as follows:

1. A backlight imaging experimental setup to acquire 2D projection images, the features of the gap beneath the relay's surface are extracted, leading to the development of a gap measurement model.
2. A surface point cloud gap measurement method based on the convex hull of the 3D surface point cloud and relay centroid projection.
3. A method based on visual information that integrates 2D and 3D measurement features is proposed, which effectively addresses the limitations of conventional gap measurement methods and enhancing measurement accuracy.

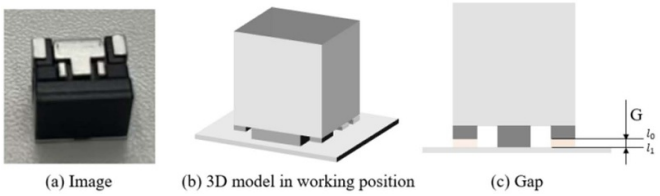


**Figure 1.** The relay and the gap.

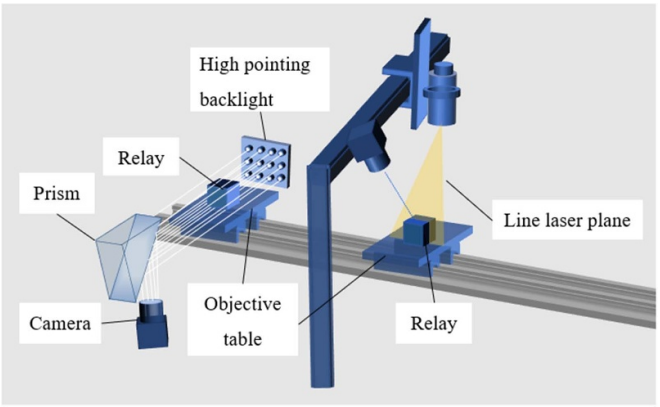


**Figure 2.** The measurement system used in this paper.

## 2. A vision-based measurement system for relays

Figure 1 shows the relay's shape, its 3D model in the working position, and the gap between the relay and ground. The relay is made of metal and plastic materials. For a qualified relay, the gap should be less than 0.07 mm in the working state. This paper presents a 2D + 3D method for detecting gaps quickly and accurately. The measuring system is shown in Figure 2, and it includes a backlight imaging system and 3D points acquisition system.

## 3. A gap measurement method based on the projection line model

### *3.1. Construction of the image acquisition system*

A backlighting acquisition scheme is developed as shown in figure 3, where high-intensity illumination creates a significant contrast between the gap and the light-blocking object. Traditional backlighting can lead to diffraction phenomena, which makes the edge imaging challenging. For this reason, a highly directional backlight source is applied to suppress the diffraction of the illuminating light, enabling clear imaging of the edges, making it more suitable for high-precision measurements.

By adjusting the relative positions of the camera, the relay and the light, the bottom edge of the relay and the edge of the ground each form a clear straight line ($l_0$ and $l_1$ in figure 1) upon achieving clear imaging. During the measurement process, the relative distance between the camera and the relay remains unchanged, establishing a linear relationship between

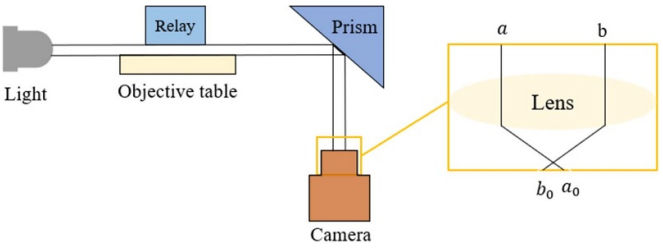


**Figure 3.** The backlighting acquisition scheme.

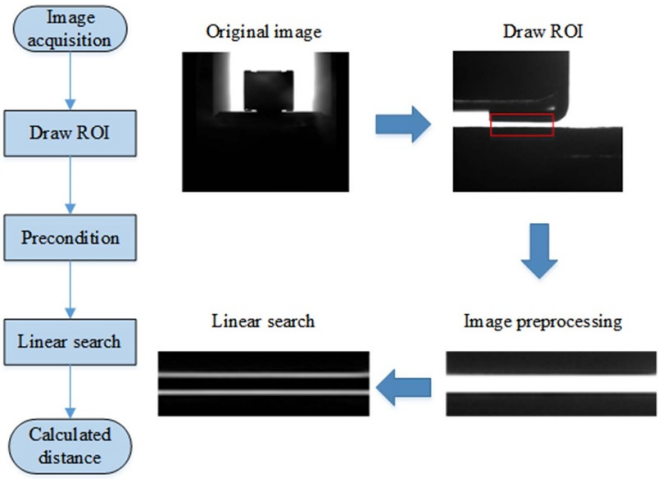


**Figure 4.** The flow chart of image processing algorithm.

the image pixel distance $b_0a_0$ and the actual distance ab in the real world:

$$\mathrm{ab} = k \times b_0a_0 \tag{1}$$

where $\boldsymbol{k}$ is a constant. To minimize errors arising from distortion and the calibration process, the paper specifically selects industrial lenses with low distortion rates.

### 3.2. 2D image processing

To achieve high-speed detection while maintaining detection accuracy, the paper designs an image processing scheme as illustrated in figure 4.

The image capture process is prone to noise due to factors such as exposure time, electronic interference, or variations in photosensitive components, necessitating the introduction of an image preprocessing phase. Guided filtering [13–15] excellently maintains edges and enhances details while smoothing image noise, avoiding the common issue of edge blurring seen with traditional filters. This process can be expressed as follows:

$$Q_i = \sum W_{ij}(I) P_j \tag{2}$$

$$W_{ij} = \frac{1}{|\omega|^2} \sum_{k:(i,j)\in\omega_k} \left(1 + \frac{(I_i - \mu_k)(I_j - \mu_k)}{\sigma_k^2 + \varepsilon}\right) \tag{3}$$

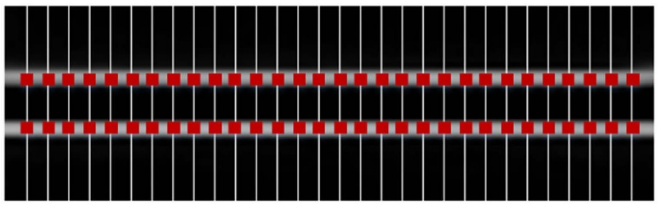

**Figure 5.** Schematic diagram of linear search algorithm.

where $\boldsymbol{I}$ is the guidance image, $\boldsymbol{P}$ is the input image to be filtered, $\boldsymbol{Q}$ is the filtered output image, and $\boldsymbol{W}$ is the weight determined by the guidance image $\boldsymbol{I}$; $\boldsymbol{\mu_k}$ represents the mean of pixel values within the window, $\boldsymbol{\sigma_k}$ represents the variance of pixel values within the window, $\boldsymbol{I_i}$ and $\boldsymbol{I_j}$ are the values of two adjacent pixels, and $\varepsilon$ is a regularization term. Usually, guided filter allows pixels in flat areas to be weighted more significantly, which results in a noticeable smoothing effect. On the contrary, pixels on the boundaries are weighted less, resulting in weaker smoothing effects and thus achieving edge preservation.

The filtered image allows for the extraction of line information via line searching, as shown in figure 5. The search lines run vertically from the top to the bottom surface of the region of interest (ROI), with pixel points serving as endpoints.

To enhance the accuracy and robustness of the gap measurement, a 3 × 3 Sobel operator [16] is applied to calculate gradient values, with coefficients as follows:

$$G_x = \begin{bmatrix} -1 & 0 & 1 \\ -2 & 0 & 2 \\ -1 & 0 & 1 \end{bmatrix} \tag{4}$$

$$G_y = \begin{bmatrix} -1 & -2 & -1 \\ 0 & 0 & 0 \\ 1 & 2 & 1 \end{bmatrix}. \tag{5}$$

Consequently, the gradients in the $x$ and $y$ directions can be calculated sequentially as:

$$\begin{aligned} G_x(x,y) = {} & f(x+1,y-1) + f(x+1,y+1) \\ & - f(x-1,y-1) - f(x-1,y+1) \\ & - 2f(x+1,y) - 2f(x-1,y) \end{aligned} \tag{6}$$

$$\begin{aligned} G_y(x,y) = {} & f(x-1,y+1) + f(x+1,y+1) \\ & - f(x-1,y-1) - f(x+1,y+1) \\ & + 2f(x,y+1) + 2f(x,y-1). \end{aligned} \tag{7}$$

Furthermore, the gradient magnitude can be determined as:

$$G = \sqrt{{G_x}^2 + {G_y}^2}. \tag{8}$$

Given that in the image, the transition between gaps and objects results in significant changes in grayscale values. By identifying the two coordinates where the gradient values are highest for each search line.

Observing the above pre-processed region of interest reveals that the relay is subject to burr defects, as shown in

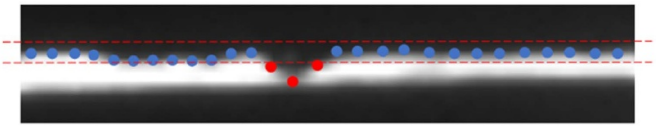

**Figure 6.** The burr defect diagram.

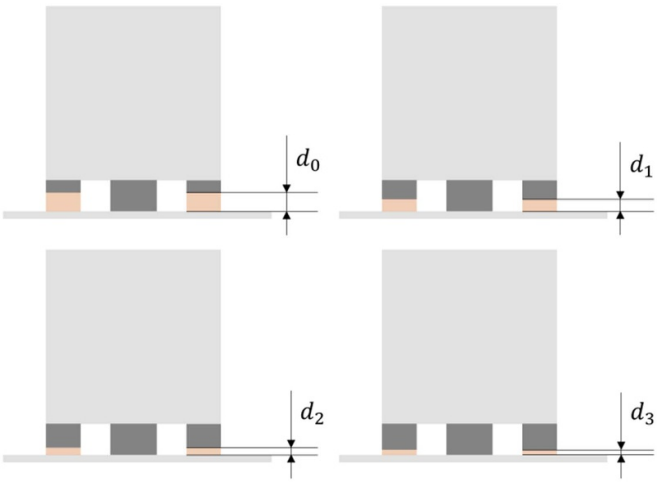


**Figure 7.** Several sample set images.

figure 6, due to limitations in the metal surface's machining process.

The paper assumes a line deviation evaluation metric, denoted as $\boldsymbol{C}$, to eliminate noise points caused by burr defects and thereby enhancing the accuracy of the fitted line.

The model for calculating the line deviation evaluation value can be described as follows:

$$\begin{aligned} P_l &= |Y_i - Y_{i-1}| \\ P_r &= |Y_{i+1} - Y_i| \\ C_i &= \begin{cases} 1, & P_l > t, P_r > t \\ 0, & \text{else} \end{cases} \end{aligned} \tag{9}$$

where $\boldsymbol{C_i}$ represents the deviation evaluation value for point $\boldsymbol{i}$ in the set, $\boldsymbol{P_l}$ and $\boldsymbol{P_r}$ are the left and right deviation distances for the point, $\boldsymbol{Y_i}$ is the vertical coordinate of point $\boldsymbol{i}$, and $\boldsymbol{t}$ is the deviation threshold. $\boldsymbol{C_i} = 1$ indicates that the point is a noise point deviating from the line, which is then excluded from the set. Subsequently, the least squares method is employed to fit a line to the denoised set of points, with the error objective function defined as:

$$E = \sum_{i=1}^{n} (y_i - mx_i - b) \tag{10}$$

where $\boldsymbol{X_i}$ and $\boldsymbol{Y_i}$ are the coordinates of points on the line, and $\boldsymbol{m}$ and $\boldsymbol{b}$ are the coefficients of the line equation. By minimizing the above expression based on the least squares criterion, the corrected line equation can be obtained.

As shown in figure 7, the pixel distance between two lines the line along the bottom surface of the relay and the baseline is calculated.

Initially, it is necessary to measure the actual gap distance $\boldsymbol{D}$ and the pixel distance $\boldsymbol{d}$ in the detected image. Subsequently, by averaging over multiple experiments, measurement errors that may occur during the process are reduced. Finally, the calibration coefficient $\boldsymbol{k}$ can be obtained:

$$k = \frac{\sum_{i=0}^{n} (D_i/d_i)}{n}. \tag{11}$$

With the calibration coefficient derived from formula (11), the pixel distance $\boldsymbol{d}$ can be accurately converted into the real distance.

## 4. Gap measurement method based on the surface point cloud model

Compared with merely 2D images, 3D point clouds can provide comprehensive information of objects. Therefore, this paper leverages the high precision and resolution characteristics of point cloud measurements to develop a novel gap measurement method based on contact surface localization. The main steps of the 3D measuring system are illustrated in figure 8.

### *4.1. Point cloud pre-processing*

As shown in figure 9, the process of acquiring depth map data with a three-dimensional camera are contaminated with outliers, due to the existence with the dark regions and shadows which leads to errors for measurement. Therefore, it is necessary to eliminate these outliers. An outliner detection and cleaning algorithm based on the number of the neighbour points are developed as following.

Firstly, this paper defines a mask for the $N$-neighbourhood and iterate over each point in the image, calculating the distance between that point and the points within its neighbourhood:

$$d_{ij} = \sqrt{(x - x_{ij})^2 + (y - y_{ij})^2 + (z - z_{ij})^2} \tag{12}$$

where $(\boldsymbol{x},\boldsymbol{y},\boldsymbol{z})$ are the actual coordinates of the point, and $(\boldsymbol{x_{ij}},\boldsymbol{y_{ij}},\boldsymbol{z_{ij}})$ are the actual coordinates of the neighboring point $(\boldsymbol{i},\boldsymbol{j})$.

Consequently, a threshold $\boldsymbol{T_1}$ is set to mark the neighbourhood points with a distance $\boldsymbol{d_{ij}}$ greater than $\boldsymbol{T_1}$ as 1 on the mask, and otherwise as 0. This mark indicates the degree of outlier status; 0 for non-outliers and 1 for outliers. A threshold $\boldsymbol{T_2}$, assess the number of outlier points in the mask corresponding to a point, where a greater number indicates a higher degree of outlier status.

$$M_{ij} = \begin{cases} 1, & d_{ij} > T_1 \\ 0, & d_{ij} \leqslant T_1 \end{cases} \tag{13}$$

$$S = \sum_{i,j \in N} M_{ij}, \tag{14}$$

where $\boldsymbol{M_{ij}}$ is the mask marking value for point $(\boldsymbol{i},\boldsymbol{j})$ in the neighbourhood corresponding to a certain point, and $\boldsymbol{S}$ is the

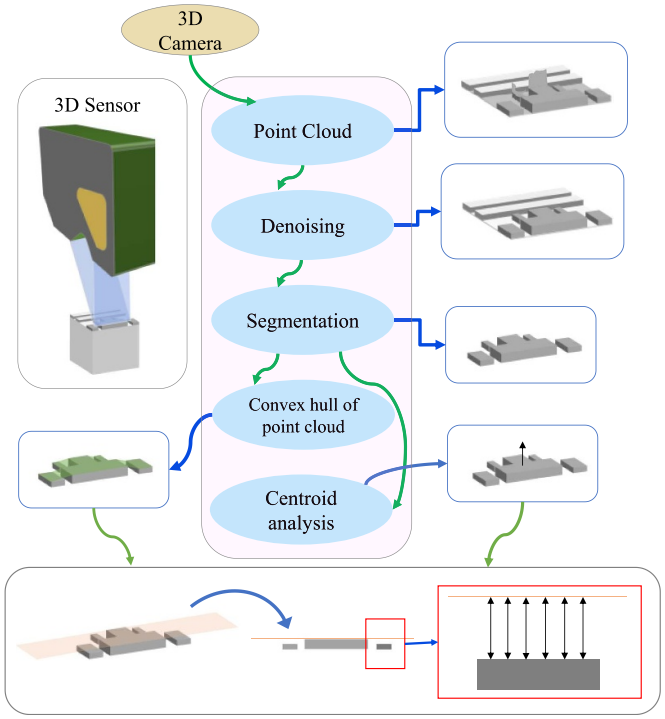


**Figure 8.** Steps (green arrows) of 3D points method proposed in this paper.

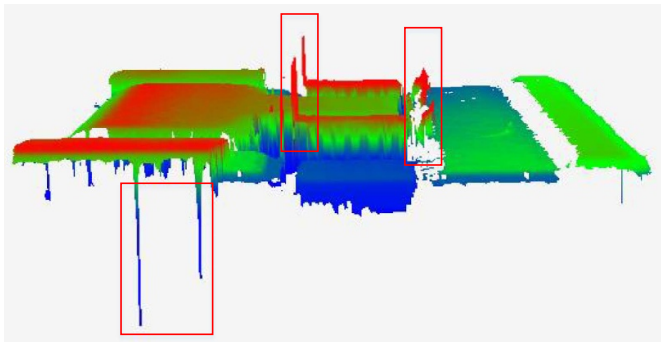

**Figure 9.** The 3D point cloud contaminated with outliners and noises.

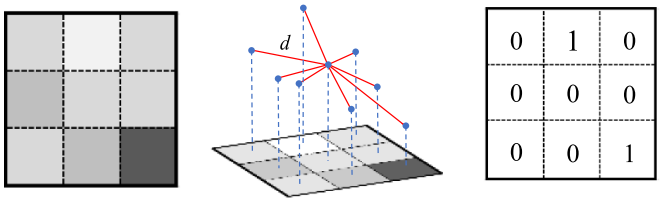


**Figure 10.** The gap measurement model based on surface point cloud.

degree of outlier status for that point. A point's degree of outlier status $\boldsymbol{S}$ exceeding the threshold $\boldsymbol{T_2}$ indicates that the point is an outlier. Figure 10 clearly illustrates this process. To accurately detect the surface gap distance, it is necessary to use a connected component segmentation algorithm [17, 18] to separate the different regions into distinct parts.

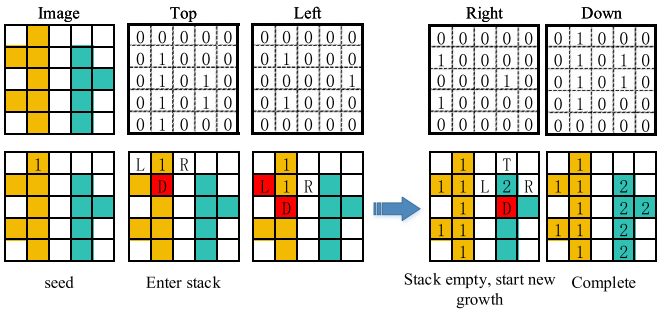


**Figure 11.** The principle of connectivity-based segmentation algorithm on the image.

The segmentation method used in this study, as illustrated in figure 11, which initially involves calculating the Top, Left, Right, and Down images using a four-neighbourhood Mask template and threshold T, namely:

$$X(i,j) = \begin{cases} 0, & |f(i,j) - f(i+m,j+n)| > T \\ 1, & |f(i,j) - f(i+m,j+n)| \leqslant T \end{cases}, \tag{15}$$

where $\boldsymbol{X}$ can be replaced by $\mathrm{Top}\,(m=-1,n=0)$, $\mathrm{Left}\,(m=0,n=-1)$, $\mathrm{Right}\,(m=0,n=1)$,$\mathrm{Down}(m=1, n=0)$, which represent the coordinate values of point $(i,j)$ in the corresponding state images, and $\boldsymbol{f}$ $(\boldsymbol{i},\boldsymbol{j})$ denotes the coordinate value of point $(i,j)$ in the original image.

Subsequently, a set of regions is constructed. Utilizing the four state images mentioned above, the entire image is traversed to allocate areas. The depletion of the stack signifies the completion of the growth of a connected region, and the corresponding position information is saved. Growth then commences from another unexplored new element, initiating a new connected region's growth. This process is repeated until all regions have been segmented. The final output was the information of the segmented regions.

### *4.2. Point cloud gap distance*

Addressing the challenges associated with the high complexity of point cloud surface fitting, where computational efficiency and fitting accuracy are difficult to guarantee simultaneously, this paper constructs a 3D surface point cloud's convex hull [19, 20] as illustrated in figure 12(d) and calculates the centroid projection of the relay to precisely locate the contact surface between the relay and the ground, thereby determining the gap distance between the relay's lower surface and the ground.

A convex hull refers to a convex polyhedron formed by connecting the outermost points in a set within a three-dimensional space, commonly used to simulate contact between objects. This paper uses the fast convex hull algorithm to find the convex hull of a point set in three-dimensional space. The steps are as follows:

Step 1: Initializing a tetrahedron composed of four vertices.

Step 2: Storing the data structure of each face $F$, then Initializing the visible sets $V$.

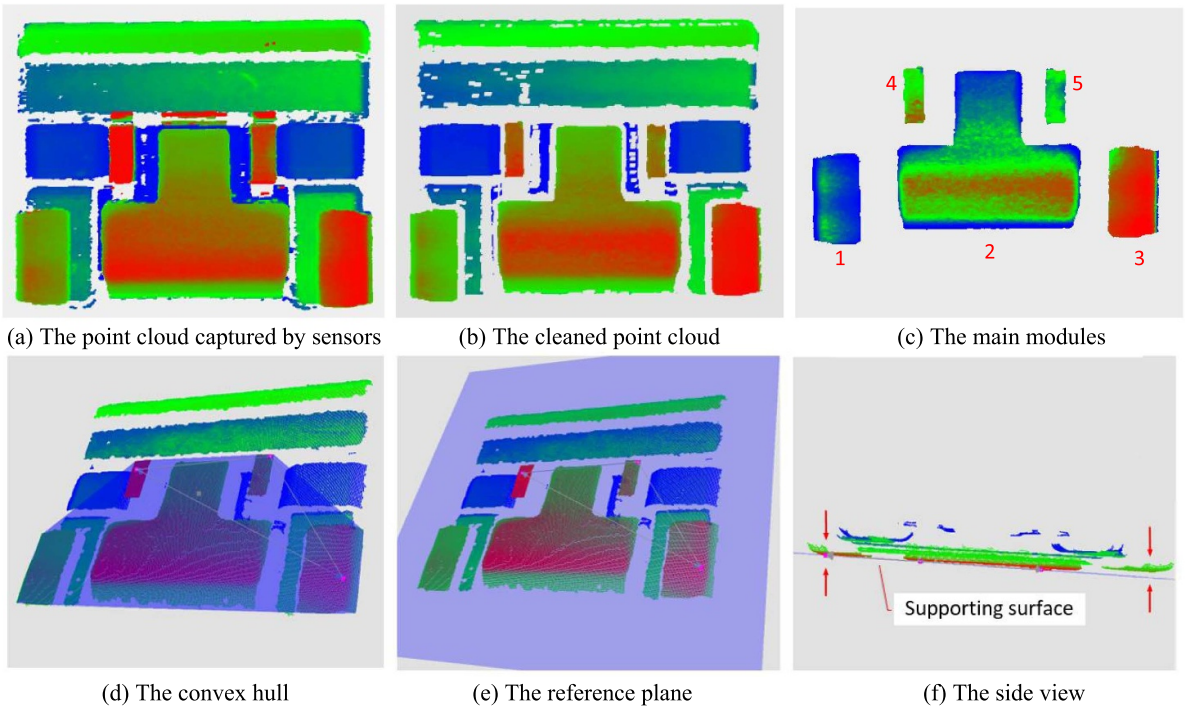


(a) The point cloud captured by sensors (b) The cleaned point cloud (c) The main modules

(d) The convex hull (e) The reference plane (f) The side view

**Figure 12.** The diagram of point cloud processing and calculation process force analysis.

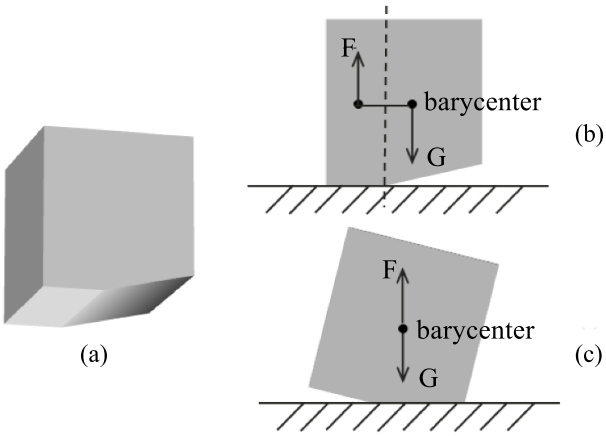


**Figure 13.** The gravity and force analysis on the object to be measured.

Step 3: Summarizing the set of external points of each face in the visible surface set into the point set $L$.

Step 4: Connecting the points in the point set $L$ and the edges in the set $V$, and creating a new surface, then updating the adjacent faces of the surface.

Step 5: If the intersection between the set $Q$ of undetermined surfaces and the set $V$ of the visible surface is not empty, then remove their intersection from the set of undetermined surfaces.

Finally, for each new surface, if its set of external points is not empty, it will be added to the set of undetermined surfaces and next iteration is started.

As illustrated in Figure 13, when an object is placed on the ground as shown in Figure 13(a), it often needs to reach a state of equilibrium under the action of rotational torque, as depicted in Figure 13(b). In contrast, as shown in Figure 13(c), when the resultant force and moment acting on the object are zero, the object can achieve a state of equilibrium. Therefore, projecting the centroid in the direction of gravity allows for the identification of the supporting surface intersecting with the convex hull.

Usually, it is not necessary for the relay to be positioned horizontally. However, it is essential to ensure that the sensor captures all potential positions of the lower surface of the relay.

To enhance the precision of its measurements, this paper employs a method that assigns different weights to the various material parts of the device to determine its centroid as follows:

$$X_G = \frac{\sum_{i=0}^{n_1}\rho_1 x_1 + \sum_{j=0}^{n_2}\rho_2 x_j + \cdots + \sum_{k=0}^{n_k}\rho_h x_k}{\sum_{i=0}^{n_1}\rho_1 + \sum_{j=0}^{n_2}\rho_2 + \cdots + \sum_{k=0}^{n_k}\rho_h} \tag{16}$$

$$Y_G = \frac{\sum_{i=0}^{n_1}\rho_1 y_1 + \sum_{j=0}^{n_2}\rho_2 y_j + \cdots + \sum_{k=0}^{n_k}\rho_h y_k}{\sum_{i=0}^{n_1}\rho_1 + \sum_{j=0}^{n_2}\rho_2 + \cdots + \sum_{k=0}^{n_k}\rho_h} \tag{17}$$

$$Z_G = \frac{\sum_{i=0}^{n_1}\rho_1 z_1 + \sum_{j=0}^{n_2}\rho_2 z_j + \cdots + \sum_{k=0}^{n_k}\rho_h z_k}{\sum_{i=0}^{n_1}\rho_1 + \sum_{j=0}^{n_2}\rho_2 + \cdots + \sum_{k=0}^{n_k}\rho_h} \tag{18}$$

where, $\boldsymbol{X_G}$, $\boldsymbol{Y_G}$, and $\boldsymbol{Z_G}$ represent the coordinate values in the $\boldsymbol{XYZ}$ directions, and $\boldsymbol{\rho}$ denotes the density of the corresponding point.

After obtaining the centroid, the support surface can be determined through projection, and the vertical distance from the points on the point cloud surface to the support surface can be calculated. Then, it will thus accurately determine the measured gap. Figures 12(a)–(f) illustrate point cloud processing and its calculation workflow.

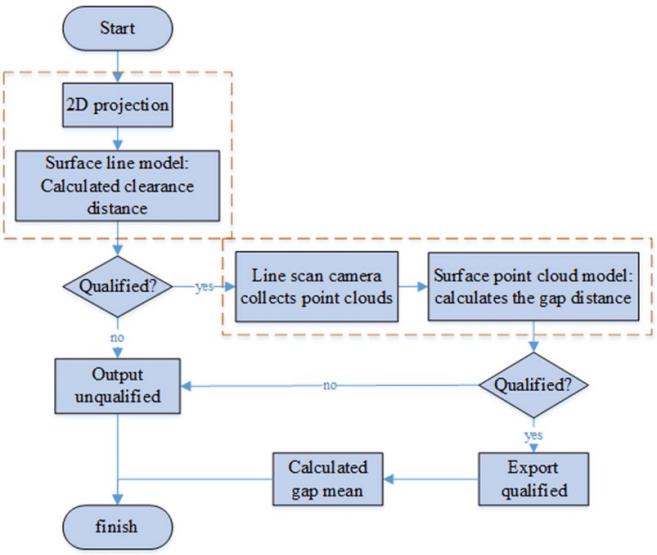


**Figure 14.** The flow chart of inspection system.

### *4.3. Measurement models include 2D and 3D*

To adapt to the real production environment and further enhance the accuracy and speed of quality inspection during the relay production process using the methods proposed in this paper, we integrated 2D and 3D models. This study aims to construct a gap detection model capable of handling various surface processing defects with rapid detection speed, high precision, and stability. Initially, the projection line detection model served as the rough detection phase of the integrated model, conducting a preliminary. Subsequently, the surface point cloud model acted as the fine detection phase, performing a second round of testing on the samples that passed the initial screening. A flowchart of the integrated model is shown in figure 14.

## 5. Experimental results and analysis

### *5.1. Experimental setup*

To verify the effectiveness and feasibility of the new method for measuring the gap beneath the surface of the relay proposed in this study, an experiment was set up as shown in Figure 15. This platform is composed of a 2D camera, line-scan laser camera, lens, high-directional backlight source, prism and relay. The detailed parameters of the onsite experimental equipment are listed in Table 1. To enhance the quality of the captured images, the focal length and exposure time of the camera were adjusted in advance. The performance of the method proposed in this paper was compared with the gap measured and calculated by methods Pixel Area [4] and SelfConvNet [4].

### *5.2. Measurement results analysis*

It is evident from the Figure 16 that the point-cloud-based measurement method proposed in this paper exhibits superior

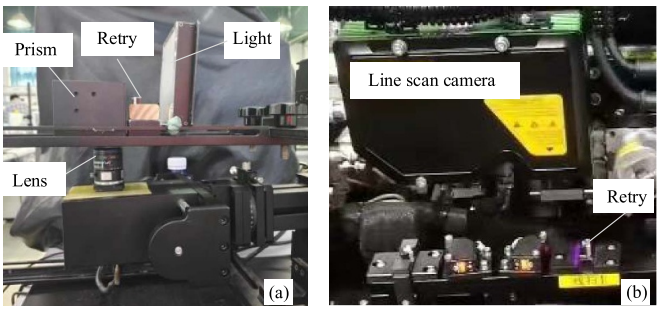


**Figure 15.** Experimental platform; (a) the 2D Projection based measure system and (b) the 3D laser profiler 3D data-based system.

linearity compared to the commonly used Pixel Area and SelfConvNet models, and the linearity of measurement model include 2D and 3D is best.

Analysis of the model principles and experimental results revealed that the Pixel Area model calculates the gap distance by projecting the gap area within the image. However, when surface defects occur on the underside of the relay, a significant discrepancy arises between the projected gap area and actual gap area, which leads to considerable fluctuations in the linearity experiment results. In contrast, the projection line model proposed in this study assesses the deviation of line points to eliminate noise points caused by burr defects, thereby reducing the impact of burr defects on measurement accuracy and resulting in better linearity than that of the Pixel Area model. The SelfConvNet model exhibits good linearity through feature extraction and training on projection images of different gap distances. However, network training is constrained by the lack of 2D image dimensions.

The surface point cloud measurement model introduced in this study, which analyses 3D data, can effectively handle various surface defects and has a strong denoising capability. Therefore, the linearity between the measurement results of this model and the actual values is significantly superior to that of the other models.

The measurement accuracy of each method was verified by sequentially setting multiple lower surface gaps (0–0.1 mm at equal distances) with the error values depicted in Figure 17. These data are measurement values of a single relay gap.

Both the projection line model and Pixel Area model exhibited an average measurement accuracy greater than +0.01 mm. The error curve of the Pixel Area measurement showed the most significant fluctuation at 0.047 mm, whereas the maximum error for the projection line method was 0.028 mm. The surface point cloud model achieved a measurement error of 0.0095 mm, with a maximum error of 0.02 mm; and the surface point cloud model achieved a measurement accuracy of 0.0087 mm, with a maximum error of 0.015 mm. The experimental results indicate that the surface point cloud model performs better in terms of both maximum and average errors. Measurement error of the proposed model include 2D and 3D are minimum, with a max error of 0.009 mm and an average error of 0.0054 mm.

**Table 1.** Technical parameters of experimental equipment.

| | | | | |
|---|---|---|---|---|
| Camera | Model number<br>OPT-CC1200-GL-04 | Resolution<br>4000 × 3000 | Pixel size /$\mu m^2$<br>1.85*1.85 | Frame rate<br>9 |
| Lens | Model number<br>OPT-COB3528B | Focus Distance /mm<br>35 | Working distance/mm<br>210 ∼ ∞ | Magnification<br>0.161X at WD 210 |
| Light source | Model number<br>OPT-FLP9090-W | Color<br>White | Power consumption<br>24 v/8 W | Light intensity<br>255 |
| 3D Sensor | Model number<br>OPT-LPE50 | Reference distance/mm<br>50 | *Z*-axis repeated accuracy/um<br>0.2 | *X*-axis repeated accuracy/um<br>7 |

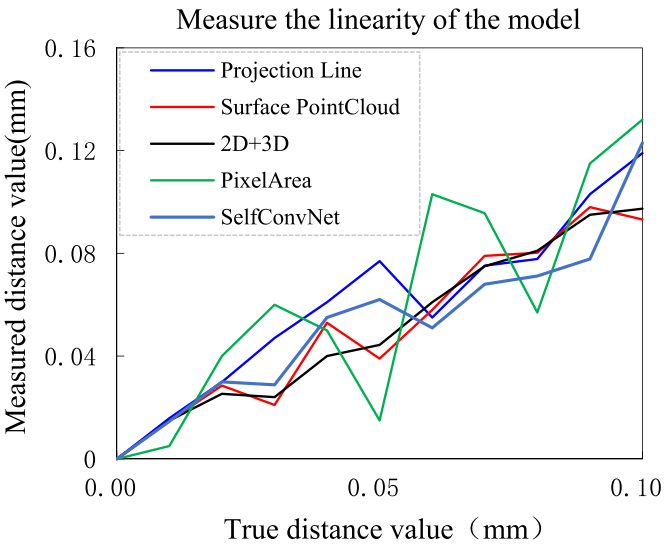


**Figure 16.** Linearity tests of different method.

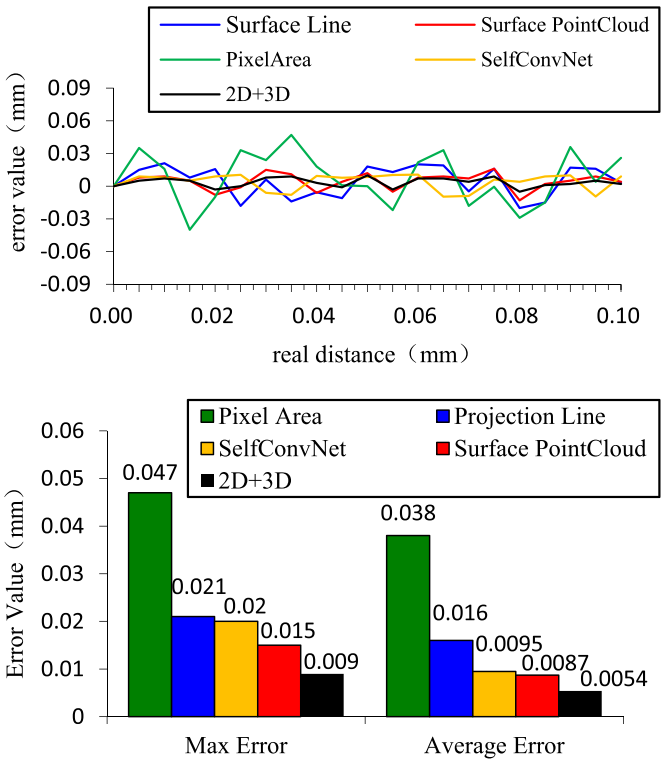


**Figure 17.** Measurement errors of different measurement methods.

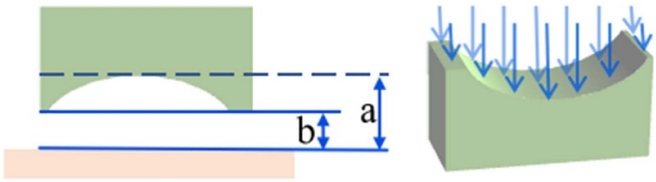


**Figure 18.** The schematic diagram of surface defect model.

To further analyze the advantages of the surface point cloud model over the other models, manual inspections were conducted on relay samples that were mis-detected under the four models. The inspection results revealed that mis-detected relay samples under each model exhibited varying degrees of surface defects, particularly pits and burrs.

Owing to limitations in surface machining processes, metal surfaces are prone to defects such as pits and burrs, which not only affect their appearance and mechanical properties, while it may also introduce safety risks during use. As shown in figure 18, the depth at the bottom of the pit corresponds to line a. However, owing to edge occlusion, the lower surface line is represented as line b in the projection image. In the experiments, the Pixel Area model, SelfConvNet model, and projection line model proposed in this paper all calculate the gap distance based on the features of the projection image. However, their detection capabilities are significantly reduced owing to the constraints of missing 2D image dimensions. In contrast, the 3D surface point cloud feature model proposed in this study can calculate the distance between the entire surface and support surface, making it less susceptible to pit defects. Therefore, this model demonstrates better performance in terms of the measurement accuracy and error range.

In summary, 2D detection methods are limited by the absence of dimensions, which usually makes it difficult to surpass the upper limit of detection accuracy, and they are also more prone to measurement errors owing to surface defects. However, these methods benefit from a relatively simple processing flow and high speed. On the other hand, 3D detection methods, due to more comprehensive input data, offer multiple and flexible processing means, high measurement accuracy,

**Table 2.** The flow chart of inspection system.

| Detection model | False drop rate | Time/ms |
|---|---|---|
| Projection line | 5% | 19.8 |
| 3D point cloud | 2% | 236.8 |
| 2D + 3D | 0.05% | 182.4 |
| Pixel Area | 6.6% | 48.5 |
| SelfConvNet | 2.6% | 510 |

and reliability, albeit at the cost of longer algorithm processing times.

This study tests the pass rate of the relay gaps and the average detection speed. The test results are listed in table 2. In this experiment, 11 931 relays were tested, including 9247 good and 2684 defective relays. The tested results indicate that the projection line method, exhibited both higher accuracy and speed than the Pixel Area model, and the surface point cloud method outperformed the SelfConvNet model in all aspects. Notably, the integrated 2D and 3D models not only achieved the highest accuracy rate, reaching 99.5%, but also surpassed both the surface point cloud and SelfConvNet models in terms of detection speed, meeting the requirements for real-time on-site detection.

Analysis of the experimental results revealed that the line point deviation value calculation model constructed in this study effectively avoids errors caused by burr defects, thereby enhancing the detection accuracy of the surface line model. Owing to outlier removal and the advantages of 3D detection, the surface point cloud model not only circumvents errors induced by burr defects, but also can accurately measure the depth of pits, exhibiting high detection accuracy within gap measurement models. Conversely, the SelfConvNet model needs to extract sufficient features for network training from the pit-like defects. However, under the combined effect of the dual detection stages, the integrated model showed improved detection speed and accuracy. These results indicate that under certain conditions, 2D detection methods possess higher accuracy but are limited by missing dimensions and surface processing defects, preventing their advantages from being fully realized when used alone. However, 3D detection methods maintain good accuracy even under relatively complex conditions with stronger stability. Therefore, integrating 2D and 3D methods, forming a complementarity of advantages, can effectively enhance the capability of the gap measurement algorithm to handle defects, accuracy, and speed of detection.

## 6. Conclusion

To address the issues of insufficient accuracy in traditional methods for measuring the gap beneath the surface of relays, this study proposes a relay gap measurement method based on 2D projection images and 3D point cloud feature models.

(1) In the 2D measurement, the study utilized high-directional backlight sources to suppress light diffraction and employed guided filtering to effectively reduce noise interference. It constructs a line point deviation index to remove noise points caused by burr defects, which effectively handles with the gap edge information and extracting edge lines, thereby improving the accuracy of gap distance measurements.
(2) In the 3D measurement, a 3D surface point cloud feature model based on the convex hull and centroid estimation was introduced. Through outlier removal and connected component segmentation, noise interference is effectively reduced and feature information is highlighted. Precise localization of the contact surface through centroid estimation and convex hull calculations effectively minimizes errors caused by inaccurate contact surface localization, thus achieving higher accuracy in gap measurements. At the same time, it realizes an organic integration of the advantages of 2D and 3D measurement methods, further enhancing the detection accuracy, robustness, and reliability.
(3) The experimental results show that the detection accuracies of the surface line model and the surface point cloud model were 95% and 98%, respectively, while the integrated 2D and 3D models achieved a detection accuracy of 99.5%. Compared to the Pixel Area model and SelfConvNet model, it exhibits superior measurement precision and speed. The measurement system developed based on the proposed method has demonstrated superior stability and robustness in the enterprise's quality inspection process.

## Data availability statement

The data cannot be made publicly available upon publication because they contain commercially sensitive information. The data that support the findings of this study are available upon reasonable request from the authors.

## Acknowledgments

This work was financially supported by various grants, including Grant 2021A1515010661 from the National Science Foundation of Guangdong, Grant No. 2020KCXTD012 from the Guangdong Provincial Project University Innovation Team, Grant 20231127143250002 from the Shenzhen Science and Technology Plan's Stable Support Plan for Universities, and Grant SZIIT2023KJ008 from School-level Scientific and Technological Projects.

## Author contributions

**Fupei Wu:** Resources, Funding acquisition, Writing—review & editing.

**Wei Pan:** Conceptualization, Project administration.

**Binfeng Jiang:** Methodology, Validation, Formal analysis, Data curation, Writing—original draft.

**Wenming Tang:** Investigation, Software.

**Shengping Li:** Supervision.

## ORCID iDs

Wei Pan https://orcid.org/0000-0002-0933-2453
Fu-pei Wu https://orcid.org/0000-0002-7161-0047

## References

[1] Beckwith T R and Mozina C J 2017 Motor bus transfer system performance testing and the search for a new transfer success criterion *IEEE Trans. Ind. Appl.* **53** 653–9
[2] Islam S N, Mahmud M A and Oo A M T 2017 Achievable sum rate analysis of relay aided overlay device to device communication among multiple devices *J. Commun. Netw.* **19** 309–18
[3] Sharma S, Kumar R, Singh A and Singh J 2020 Wireless information and power transfer using single and multiple path relays *Int. J. Commun. Syst.* **33** 1–15
[4] Jing Y Z, Ma X C, Zhang Z F, Li Y and Kong J 2022 Research on visual measurement for levitation gap in Maglev system *IEEE Trans. Ind. Electron.* **69** 8377–86
[5] Qu Z L *et al* 2023 High-precision resistivity measurement of silicon wafer under unstable lift-off distance using inductive and laser sensors-integrated probe *IEEE Trans. Instrum. Meas.* **72** 1–8
[6] Pu M H, Zhang J H, Yao Q H, Cai B and Luo Z 2023 A calculation method for the optimal initial polar distance of capacitive force sensors *IEEE Sens. J.* **23** 6581–8
[7] Wu J, Wen B, Zhang Q, Zhou Y, Ding S, Du F, Zhang S and Wang Z 2020 A novel blade tip clearance measurement method based on event capture technique *Mech. Syst. Signal Process.* **139** 1–16
[8] Srimontriphakdi T, Mahasuwanchai P and Athisakul C 2023 A non-contact approach for cable tension evaluation based on 3D laser scanning data and nonlinear finite element analysis *Measurement* **212** 1–15
[9] Cupec R, Vidović I and Filko D 2020 Object recognition based on convex hull alignment *Pattern Recognit.* **102** 1–19
[10] Fan J F, Yang J, Zhao Y T, Ai D, Liu Y, Wang G and Wang Y 2017 Convex hull aided registration method (CHARM) *IEEE Trans. Vis. Comput. Graph.* **23** 2042–55
[11] Yan T T, Wang Y T, Xia T B, Hou B, Xi L and Wang D 2023 Sparse and flexible convex-hull representation for machine degradation modeling *IEEE Trans. Reliab.* **72** 27–36
[12] Norris J E, Clayton S, Gilmore C, Inglis M and Castronovo J 2019 The measurement of approximate number system acuity across the lifespan is compromised by congruency effects *Q. J. Exp. Psychol.* **72** 1037–46
[13] Qiao Z L, Wen X, Zhou X Y, Qin F, Liu S, Gao B, Liu W, Chi D and Liu Z 2023 Adaptive iterative guided filtering for suppressing background noise in ptychographical imaging *Opt. Lasers Eng.* **160** 107233
[14] Guo X J, Li Y, Ma J Y and Ling H 2020 Mutually guided image filtering *IEEE Trans. Pattern Anal. Mach. Intell.* **42** 694–707
[15] Singh H, Kommuri S V R and Kumar A 2021 A new technique for guided filter-based image denoising using modified cuckoo search optimization *Expert Syst. Appl.* **176** 1–22
[16] Jing M and Du Y B 2021 Flank angle measurement based on improved Sobel operator *Manuf. Lett.* **25** 44–49
[17] Wrasse A D, Dos Santos E N, da Silva M J, Wu H and Tan C 2022 Capacitive sensors for multiphase flow measurement: a review *IEEE Sens. J.* **22** 21391–409
[18] Yu Y, Wang C P, Fu Q, Kou R, Huang F, Yang B, Yang T and Gao M 2023 Techniques and challenges of image segmentation: a review *Electronics* **12** 1199–222
[19] Linh N K, An P T and Hoai T V 2022 A fast and efficient algorithm for determining the connected orthogonal convex hulls *Appl. Math. Comput.* **429** 127183
[20] Guo Z H, Zhang X S, Liu C, Ji X, Jiao J and Ye Q 2022 Convex-hull feature adaptation for oriented and densely packed object detection *IEEE Trans. Circuits Syst. Video Technol.* **32** 5252–65